Mechanisms of Wave Fractionation at Boundaries of High-Frequency Excitation in the Posterior Left Atrium of the Isolated Sheep Heart During Atrial Fibrillation

Jérôme Kalifa, MD*; Kazuhiko Tanaka, MD*; Alexey V. Zaitsev, PhD; Mark Warren, PhD; Ravi Vaidyanathan, MS; David Auerbach, MS; Sandeep Pandit, PhD; Karen L. Vikstrom, PhD; Robert Ploutz-Snyder, PhD; Arkadzi Talkachou, MS; Felipe Atienza, MD, PhD; Gérard Guiraudon, MD; José Jalife, MD; Omer Berenfeld, PhD

Background—High-frequency fractionated electrograms recorded during atrial fibrillation (AF) in the posterior left atrium (PLA) and elsewhere are being used as target sites for catheter ablation. We tested the hypothesis that highly periodic electric waves emerging from AF sources at or near the PLA give rise to the most fractionated activity in adjacent locations.

Methods and Results—Sustained AF was induced in 8 isolated sheep hearts (0.5 μmol/L acetylcholine). Endocardial videoimaging (DI-4-ANEPPS) and electric mapping of the PLA enabled spatial characterization of dominant frequencies (DFs) and a regularity index (ratio of DF to total power). Regularity index showed that fractionation was lowest within the area with the maximal DF (DFmax domain; 0.19 ± 0.02) and highest within a band of $\approx$3 mm (0.16 ± 0.02; $P=0.047$) at boundaries with lower-frequency domains. The numbers of spatiotemporal periodic episodes (25.9 ± 2.3) and rotors per experiment (1.9 ± 0.7) were also highest within the DFmax domain. Most commonly, breakthrough waves at the PLA traveled toward the rest of the atria ($76.8\pm8.1\%$ outward versus $23.2\pm8.1\%$ inward; $P<0.01$). In both experiments and simulations with an atrial ionic model, fractionation at DFmax boundaries was associated with increased beat-to-beat variability of conduction velocity and directionality with wavebreak formation.

Conclusions—During stable AF, the PLA harbors regular, fast, and highly organized activity; the outer limit of the DFmax domain is the area where the most propagation pattern variability and fractionated activity occur. These new concepts introduce a new perspective in the clinical use of high-frequency fractionated electrograms to localize sources of AF precisely at the PLA and elsewhere. **(*Circulation*. 2006;113:626-633.)**

Key Words: atrium ■ fibrillation ■ Fourier analysis ■ mapping

Catheter ablation for atrial fibrillation (AF) was focused initially on pulmonary vein (PV) isolation.[1,2] More recently, various alternative ablative strategies, surgical or those that use radiofrequency catheter delivery at or near the posterior wall of the left atrium (LA), have proved successful.[1,3–6] In particular, 2 studies have emphasized the possibility of using frequency and fractionation analyses of intra-atrial electrograms as guidance for ablation of AF sources.[6,7] The justification for such studies is the apparent disruption of the AF substrate associated with assumed dominant rotors in the LA and right atrium as suggested by high-frequency complex fractionated atrial electrograms (CFAEs) during mapping of AF.[6] CFAEs were found in several areas of the atria but were confined primarily to the interatrial septum, PVs, and LA roof.[6] However, the relation between local frequency, AF wave propagation patterns, and electrogram fractionation was not adequately explored.

Clinical Perspective p 633

Previously, we introduced the technique of dominant frequency (DF) mapping to characterize the spatial distribution of excitation frequencies during AF.[8,9] This approach allowed accurate identification of sites of periodic activity and the demonstration that stable, localized, high-frequency sources were responsible for AF maintenance in the isolated sheep heart. The highest DF was most often (80%) localized to the posterior LA (PLA), near or at a PV ostium. In addition, using high-resolution videoimaging, we demonstrated that such sources corresponded to fast vortexlike reentry around minuscule cores (microreentry)[8] that resulted in a large dispersion of frequencies throughout the atria during AF. Importantly, the areas

Received July 12, 2005; revision received November 17, 2005; accepted December 2, 2005.

From the Institute for Cardiovascular Research, Department of Pharmacology, SUNY Upstate Medical University, Syracuse, NY (J.K., K.T., A.V.Z., M.W., R.V., D.A., S.P., K.L.V., R.P.-S., A.T., J.J., O.B.); Hospital General Universitario Gregorio Marañón, Madrid, Spain (F.A.); and Canadian Surgery Technologies and Advanced Robotics, University of Western Ontario, London, Ontario, Canada (G.G.).

*Drs Kalifa and Tanaka contributed equally to this article.

The online-only Data Supplement can be found at http://circ.ahajournals.org/cgi/content/full/113/5/626/DC1.

Correspondence to Omer Berenfeld, PhD, Institute for Cardiovascular Research, SUNY Upstate Medical University, 750 E Adams St, Syracuse, NY 13210, E-mail berenfeo@upstate.edu

Circulation **is available at http://www.circulationaha.org** **DOI: 10.1161/CIRCULATIONAHA.105.575340**

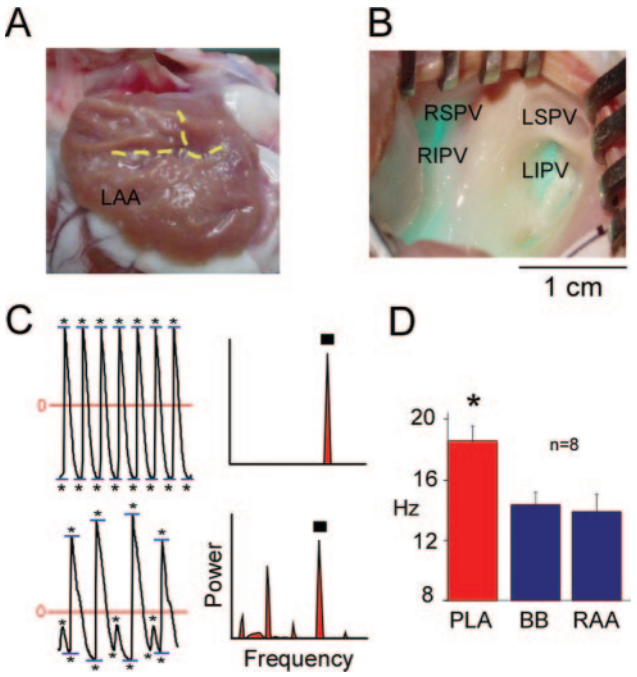

Figure 1. Atrial preparation and fractionation analysis. A, LA free wall with lines of incision. B, Exposure of the mapped PLA. The 4 PV ostia are visualized. C, Diagram of fractionation analysis. Left, Traces with horizontal lines marking the most positive and negative amplitudes used to calculate COVAMP; asterisks indicate deflections used for DFL calculation. Right, Power spectra with DF values (■) and total power (red area under the curves) used for RI calculation (DF power/total power). D, Maximal DF at PLA, BB, and RAA. RSPV indicates right superior PV; RIPV, right inferior PV; LSPV, left superior PV; and LIPV, left inferior PV. *P=0.005 vs BB and RAA.

harboring the microreentrant sources were shown to be highly regular[10] and spatiotemporally organized.[11] Fractionated activity and complex electrograms were identified mainly at boundaries separating different frequency domains,[12] eg, between the area of 1:1 activation by the microreentrant source and a neighboring lower-frequency domain. Here, we analyze optical and electrogram recordings at the endocardial surface of the PLA of the isolated sheep heart to provide insight into the mechanisms underlying high-frequency CFAEs during AF.[6] We tested the hypothesis that highly periodic electric waves emerging from AF sources at or near the PLA give rise to the most fractionated activity in adjacent locations, which would explain the relatively high success of using CFAEs to guide AF ablation therapy.

Methods

Isolated Heart Preparation

Animals were used according to NIH guidelines. Eight sheep (15 to 25 kg) were anesthetized with sodium pentobarbital (35 mg/kg IV). Hearts were removed, placed in cold cardioplegic solution, connected to a Langendorff apparatus, and continuously perfused at 200 mL/min with 36°C to 38°C Tyrode's solution (pH 7.4; 95% O_2, 5% CO_2). A minimal surgical cut was made in the LA appendage (LAA), avoiding any visible coronary branches. In Figure 1A, the lines of incision are shown in a representative example. In Figure 1B, the mapped area includes the 4 PV ostia and their junction with the endocardial wall of the PLA.

Fibrillation and Mapping

Sustained AF (>5 minutes) was induced by burst pacing in the continuous presence of acetylcholine (0.5 μmol/L) in the perfusate. An area of ≈5 cm^2 of the endocardial surface of the PLA was mapped with a CCD camera (128×128 pixels, 300 frames per second, 5-second movies) and a potentiometric dye (DI-4-ANEPPS) as detailed elsewhere.[11] We obtained 1 movie per minute for 5 minutes for every experiment. For validation, in 2 experiments (7 and 8), we also recorded bipolar electrograms from the PLA immediately after (experiment 7) or simultaneously with (experiment 8) the optical movies. In addition, in all experiments, bipolar electrograms were recorded continuously from the septal portion of Bachmann's bundle (BB) and at the right atrial appendage (RAA).

Spectral and Fractionation Analyses

Spectral and fractionation analyses of optical and electric signals were performed on their power spectra obtained by a fast Fourier transformation. A DF corresponding to the highest peak in the power spectrum in the range of 1 to 30 Hz and with a resolution of ≈0.24 Hz was determined for each signal. Thus, the DFs of all pixels were used to generate a DF map of the field of view for each movie. Thereafter, the 6 DF maps of each movie in an experiment were superimposed to construct an averaged color-coded DF map for that experiment.[12] The average map included all DF values between 1 and 30 Hz. The area with the maximal DF (DFmax domain) was defined as the area corresponding to the highest DF in that map. Boundary of DFmax was set as (DFmax-1). In addition, the power spectrum was used to quantify the fractionation of the signals, as shown in Figure 1C (right). For each signal, a regularity index (RI) was defined as the ratio of the power at the DF to total power.[13] The power at the DF was calculated by summing the power values at the highest peak and its adjacent values (fixed band of ≈0.75 Hz), and the total power was calculated as the sum over the range of 1 to 30 Hz. Average maps of RI were constructed like the DF maps. Furthermore, conventional parameters of signals variability and complexity describing fractionated activity were quantified for each pixel in each movie as follows. Movies were band pass filtered at 1 to 30 Hz. As illustrated in Figure 1C (left), for each pixel, we subtracted the average value of the signal. The time markers of the zero crossing on the fluorescent signal indicated the span of the positive and negative halves of the action potentials (APs). The amplitude of each AP was assigned on the basis of the difference between the most positive and most negative fluorescence values for each half above and below the zero line (Figure 1C, short horizontal lines). The number of deflections (DFLs; asterisks) was counted as the number of changes in slope in each half. For example, in the top tracing of Figure 1C (left), each half has 1 change in slope (positive to negative or vice versa) between its zero-crossing flanking points, whereas in the bottom tracing, the number of changes in slope is >1 for some halves. Then, the variability of the signal was quantified as the coefficient of variation in amplitude (COVAMP; SD/mean amplitude), and the complexity of the signal was quantified as the average DFL per impulse. In 6 movies per experiment, we compared the values of RI, COVAMP, and DFL inside and outside the DFmax area.

Propagation Pattern Analysis

The number, patterns, and locations of spatiotemporally periodic waves and of rotating waves were evaluated. Details of the analysis are presented in the online-only Data Supplement.

Directionality Analysis

The directionality of activation was analyzed for each pixel as follows. All activation times were determined at 50% of the upstroke of the optical AP. The vector bilinear best fit was used on a 5×5-pixel window (≈1.25×1.25 mm^2) to obtain the directions of propagation in 30° bins.[14] The recurrence of the predominant direction (RPD) was calculated from the ratio of the number of activations in the predominant direction to the total number of activations.[14]

Computer Simulations

We used a 5×5-cm^2 model with realistic atrial kinetics with heterogeneous $I_{K,ACh}$ density in the presence of 0.1 μmol/L acetylcholine.[15] Details of the model are presented in the online-only Data Supplement.

Statistical Analysis

To compare RI, COVAMP, and DFL values for regions inside and outside the DFmax area (see Spectral and Fractionation Analysis

section), the data were submitted to a 2 (region; inside or outside)×6 (time; T1 through T6) dependent-measures ANOVA, setting 2-tailed α to 0.05. We anticipated significant region differences, nonsignificant time effects, and no significant region-by-time interaction effect, confirming our hypothesis that the region effects are consistent and uniform over the 5-minute time span. We used Mauchley's test of sphericity on our repeated observations and interpreted Huynh-Feldt–adjusted significance values in cases in which our data required corrections for nonsphericity. Frequency data also were compared by use of a dependent-measures ANOVA, with 2-tailed α=0.05. In this analysis, we used a priori contrasts comparing frequency data in the DFmax area with those in the BB and RAA regions. Our comparisons of predominant wave directions also used a dependent-measures ANOVA statistic with a priori contrasts comparing the most dominant direction to the second- and third-most-dominant directions.

Results

Posterior LA Harbors the Highest DF

Figure 1D shows that in 8 experiments the DFmax was significantly higher at the PLA endocardium than at the BB and RAA (18.6±1.0 versus 14.3±0.8 and 13.9±1.2 Hz, respectively). Indeed, ANOVA comparisons supported our prediction of higher frequencies at the PLA. The overall effect was significant (P<0.006), and more importantly, a priori contrasts comparing PLA with BB and RAA DFmax values were also significant (P<0.006 and P<0.007, respectively). Notably, those DFmax values were consistent with those obtained previously in intact isolated hearts with epicardial recordings,[8,9,11,16,17] indicating appropriate perfusion conditions.

Rate and Regularity in the PLA

Average DF maps were obtained from 6 movies (5 minutes of AF) for each of the 8 experiments. In general, the pixels with DFmax (red end of the color scale; see Figure 2) spanned >36±10% of the field of view in the PLA (1.8±0.5 cm^2 of ≈5 cm^2). On average, the DFmax domain extended over 1.75±0.25 PV ostia (range, 1 to 3; left inferior PV, 6 of 8 experiments; left superior PV, 5 of 8; RIPV, 2 of 8; and right superior PV, 1 of 8).

In Figure 2A, we present 3 single-pixel optical APs, along with their power spectra. Figure 2B shows the corresponding DF (left) and RI (right) maps. The APs were obtained from 3 different areas within the highest-frequency domain (red) in which a spatiotemporally periodic wave occurred as a breakthrough at the site of highest RI (pixel 1). Thus, all 3 locations show the same dominant frequency (≈20 Hz) in their power spectra. However, as clearly illustrated in the RI map (Figure 2B, right), the 3 showed appreciably different degrees of AP fragmentation from the center to the periphery of the DFmax domain. Location 1 (red) was the most regular, followed by 2 and then 3. This was reflected by the presence of additional frequency peaks in the power spectra and lower RI values in locations 2 and 3. Thus, during stable AF, the highest degree of fractionation of the optical signal occurs at the edge of the highest-frequency domain.

To determine whether a similar relationship between local frequency and regularity could be identified through electric rather than optical recordings, we placed bipolar electrodes at locations 1 through 3 in the same experiment as that shown in Figure 2. The electrograms illustrated in Figure 2C were obtained about 20 minutes after the optical movies. At this time, all 3 bipolar electrograms showed a slightly lower frequency (≈16 Hz) than before. However, the spatial distribution of regularity was qualitatively and quantitatively the same as that shown by the earlier optical recordings. Again, location 1 shows the highest RI, with gradual reductions toward locations 2 and 3. Similar results were obtained in another experiment (data not shown), in which optical and bipolar electrogram data were obtained simultaneously. Comparison of 2 locations showed that the values of DF were similar with both techniques (17.6 and 13.7 Hz for optical and 16.9 and 14.9 Hz for electric for locations 1 and 2, respectively). The RI values were higher at the high-DF location (0.9 and 0.58 for optical and electric, respectively) than at the low-DF location (0.4 in both optical and electric). As confirmed below, a striking common feature in all our experiments is that the area of the DFmax always encompasses the highest-RI signals at the PLA.

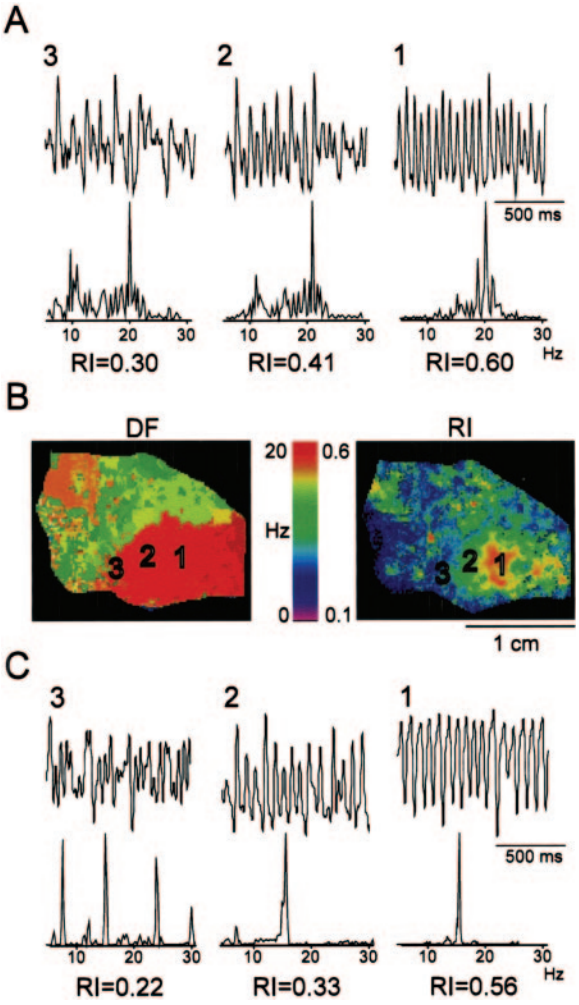

Figure 2. Optical and electrogram fractionation. A, Representative pixel recordings at locations 1, 2, and 3 (right to left). B, DF (left) and RI (right) maps for the same movie. C, Simultaneous bipolar electrograms obtained 20 minutes after optical recording at sites 1, 2, and 3. Note a similar increase in fractionation (ie, a decrease in RI) in both optical and electric signals from locations 1 to 3.

Patterns of Propagation

We quantified the properties of waves traveling in the DFmax domain to determine its role in the maintenance of AF.[8,18] In Figure 3A, 3 sequential isochronal maps show highly periodic activity emanating as a breakthrough and propagating from

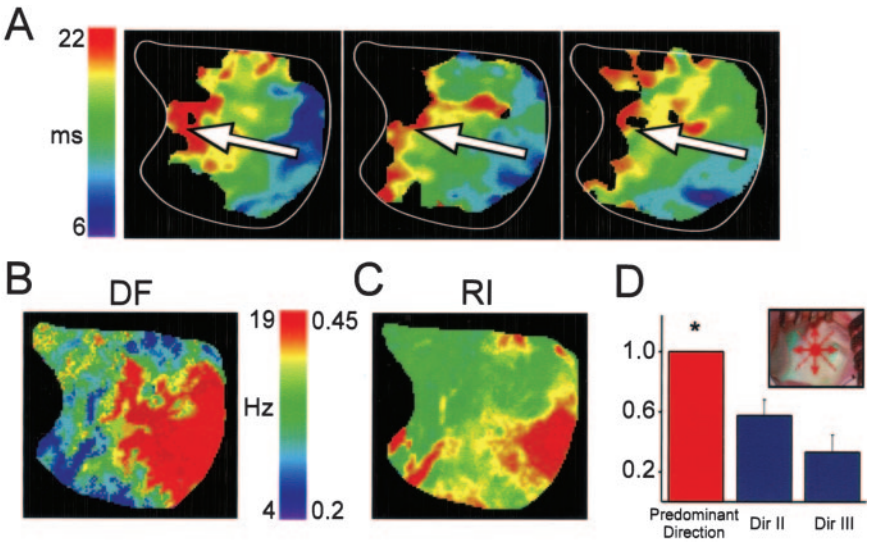

Figure 3. Recurrence in AF wave directionality. A, Consecutive activation maps showing a spatiotemporally periodic wave propagating from left PVs to the rest of the PLA (white arrows). B, Average DF map. C, Average RI map. Area of highest RI is enclosed in the DFmax domain. RI diminishes along the predominant direction of AF wave propagation. D, Wave-by-wave directionality analysis of breakthroughs at the PLA. Breakthroughs were classified according to direction (see inset and text). For each direction, the number of waves is normalized to the number at the preferential direction in each experiment. *$P<0.03$ and $P<0.009$ vs directions (Dir) II and III, respectively.

the fastest and most regular region on the right side of the field of view (lateral; dark blue) toward the left side (septal; red). As shown by the DF and RI maps in Figure 3B and 3C, respectively, the septal side demonstrated slower and more fractionated activity. In every experiment, a dominant propagation pattern could be identified on the PLA, resulting in high spatiotemporal organization. Therefore, in Figure 3D, a wave-by-wave directionality analysis was carried out after classifying the breakthrough waves as traveling in any of the 4 major directions (see inset). Comparing the number of waves in each direction in 8 experiments, an ANOVA comparison of the 3 most dominant wave directions revealed a significant overall effect ($P<0.002$), and a priori contrasts showed that direction I had a significantly higher number of waves than either direction II or III ($P<0.03$ and $P<0.009$, respectively). Overall, the average number of independent spatiotemporally periodic waves was 25.9±2.3, and the average total number of rotors lasting >1 rotation was 1.9±0.7 per experiment, each of them lasting 1.5±0.1 rotations. The most common pattern of activation was that of breakthroughs generating impulses traveling from the PLA toward the rest of the atria (76.8±8.1% traveling outward versus 23.2±8.1% traveling inward; $P<0.01$).

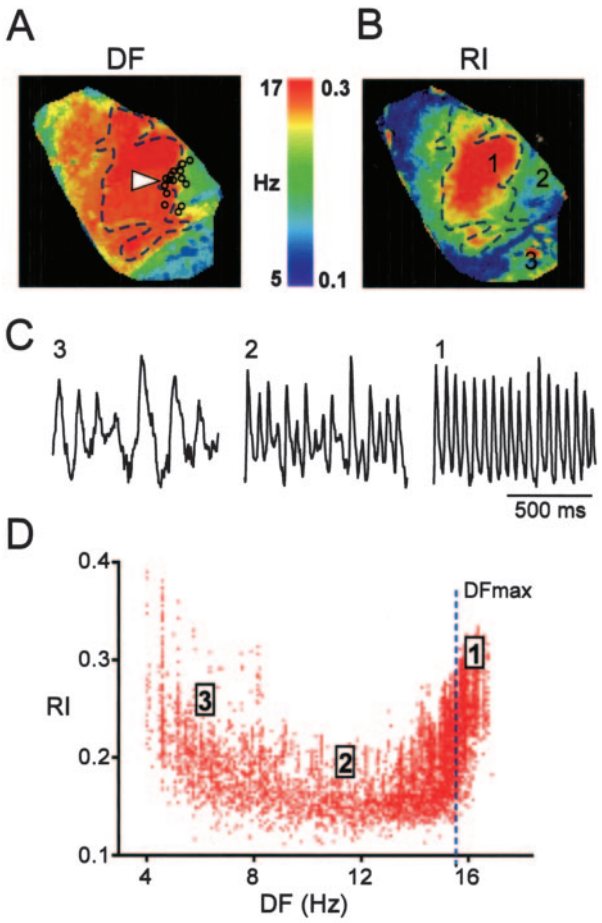

Figure 4. Relation between frequency and fractionation. A, Average DF map. B, Average RI map. C, Signals from locations 1 to 3. D, Biphasic relationship between DF and RI. Dashed line indicates limit of DFmax domain; arrowhead, predominant direction of propagation.

Local Activation Rate and Fractionation

Pixel-by-pixel quantification of the local RI enabled us to determine the spatial relation between DF and regularity. Figure 4A and 4B shows the DF and RI maps, respectively, from 1 experiment. The outline of the outer boundaries of the DFmax allows clear appreciation of the high RI inside the DFmax. RI decreases very rapidly at the boundaries of the DFmax domain but then increases again toward the periphery of the field of view. This is confirmed by the single-pixel recordings sampled from 3 different regions (points 1, 2, and 3). Although the activation frequency decreases from point 1 to 2 and then 3, RI decreases from point 1 to 2 but then increases at point 3, which corresponds to the lowest DF among all 3 points. Figure 4C depicts the relation between DF and RI for all pixels in the same experiment. A clear biphasic relation is observed. The vertical dashed line corresponds to the DFmax boundary. It indicates that the minimum RI, ie, the maximum fractionation, occurs at frequencies below the DFmax. At very low frequencies, RI again increases.

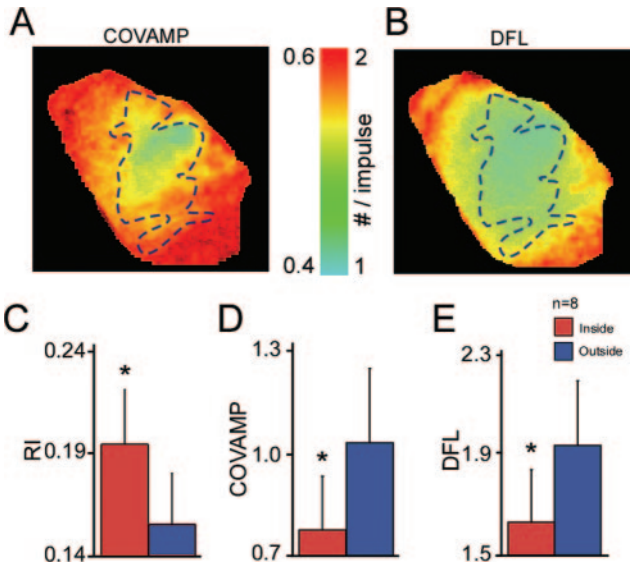

Figure 5. Signal fractionation parameters. A, Average COVAMP map. B, Average DFL map. COVAMP and DFL are minimal inside the DFmax domain (dashed line; same experiment as in Figure 4). C–E, In 8 experiments, average RI values were significantly higher inside than outside the DFmax domain (*P=0.047). The reverse was true for COVAMP and DFL (*P≤0.004).

Impulse Variability and Fractionation

We also used standard parameters of signal fractionation to quantify the variability in the amplitude of the optical signals and their DFLs. Figure 5 presents maps of 5-minute average COVAMP (Figure 5A) and DFL (Figure 5B) from the same experiment as in Figure 4. The superimposed DFmax outline adapted from Figure 4A demonstrates that both COVAMP and DFL are higher outside than inside the DFmax area. As such, COVAMP and DFL values were negatively correlated with both RI values (R=−0.17 and R=−0.10; P<0.05 and P<0.01, respectively) and DF values (R=−0.37 and R=−0.32; P=0.05 and P=0.09, respectively). Figure 5C and 5D shows quantitative data for 8 experiments. Analysis of RI, COVAMP, and DFL establishes that the degree of fractionation of the AF signals is smallest inside the fastest-activating region of the PLA. We observed significantly higher RI, lower COVAMP, and lower DFL inside than outside the DFmax area (RI, 0.19±0.03 versus 0.15±0.02, P=0.047; COVAMP, 0.81±0.19 versus 1.08±0.22, P<0.004; DFL, 1.67±0.22 versus 2.09±0.22, P=0.004 [mean±SE]). Confirming our hypotheses, the 2 (region)×6 (time) ANOVAs on RI, COVAMP, and DFL outcomes revealed only significant region effects, with nonsignificant time effects and no region-by-time interaction effects, indicating that region differences are consistent over time (see Statistical Analysis).

Fractionation and Impulse Propagation

The incidence of wavebreaks and directionality at each pixel were measured as illustrated in Figure 6. Figure 6A shows a DF map in which the outer limit of the DFmax area is outlined by the dashed curve and the general direction of wave propagation (arrow) is outward of that domain. Singularity points corresponding to sites of wavebreaks also are noted (circles) and seen to cluster primarily on an ≈3-mm rim around the DFmax domain, ie, where RI is minimal. In all experiments, 92.1±3% singularity points localized within that

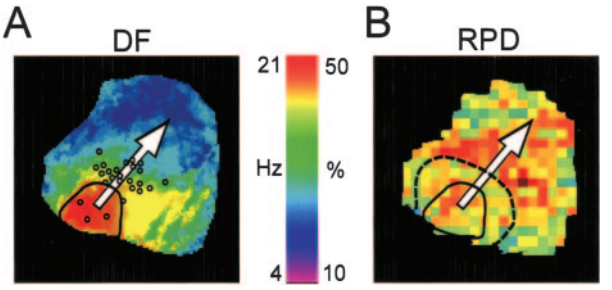

Figure 6. Pixel-by-pixel directionality analysis. A, DF map. B, Average RPD map for the same experiment shows sharp decrease of RPD around the limit of DFmax domain. Inner solid line indicates limit of the DFmax domain. Area between the solid and dashed lines shows low RPD. Arrow shows the general direction of wave propagation; circles, phase singularities corresponding to wavebreak sites.

rim. Figure 6B shows an average map, color-coded for percentage recurrence of local predominant direction (RPD; see Material and Methods). Here, the inner solid line shows the limit of the DFmax domain; the outer dashed line limits the area of low RPD. Although on average the RPD was not different between inside and outside the DFmax area (33.8±0.9% versus 32.8±0.6%; P=NS), in 5 of 8 experiments, it was possible to identify a rim at the outer limit of the DFmax frequency domain in which the direction of propagation changed more frequently on a beat-to-beat basis than elsewhere. This rim coincided with the area of lowest RI.

Computer Simulations

To provide additional insight into the mechanisms underlying local fractionation during AF without the confounding effects of the complex atria, we used a numerical approach. Figure 7A shows a snapshot of a simulation in a 2D sheet. Stable reentry in the upper half of the sheet acted as the high-frequency source of fibrillatory waves that propagated toward the bottom of the sheet with a slightly different angle on the right and left sides of the sheet (see movie in the online-only Data Supplement). The DF map in Figure 7B, corresponding to 4 seconds of simulation, shows 3 frequency domains: In the upper half, a 21.7-Hz frequency domain (DFmax) matches the rotor frequency; in the lower half, domains of 13.2 and 12.7 Hz reflecting complex propagation patterns were identified. In Figure 7C, except for the center of rotation, the highest-RI region coincides with the DFmax domain. Figure 7D shows a profile of RI along the vertical line in Figure 7C. It reveals an area of very low regularity along a narrow band between the DFmax and the lower-DF domains. This correlates highly with the AP recordings in Figure 7E, obtained from locations 1 through 4 in the sheet. Clearly, activity in the DFmax domain is highly organized, whereas fragmentation (low RI) occurs at the boundary with the lower-frequency domains. Concomitantly, the phase singularities were clustered close to the limit between DFmax and low-DF domains (see Figure 7C). However fragmentation is again reduced (ie, increased RI) at the low-frequency domain, distant from the interface with the DFmax domain.

In Figure 8, we present 15 consecutive local activation maps from 3 sites during the same simulation. Figure 8A shows activation maps from site 1 where directionality is highly recurrent (RPD,

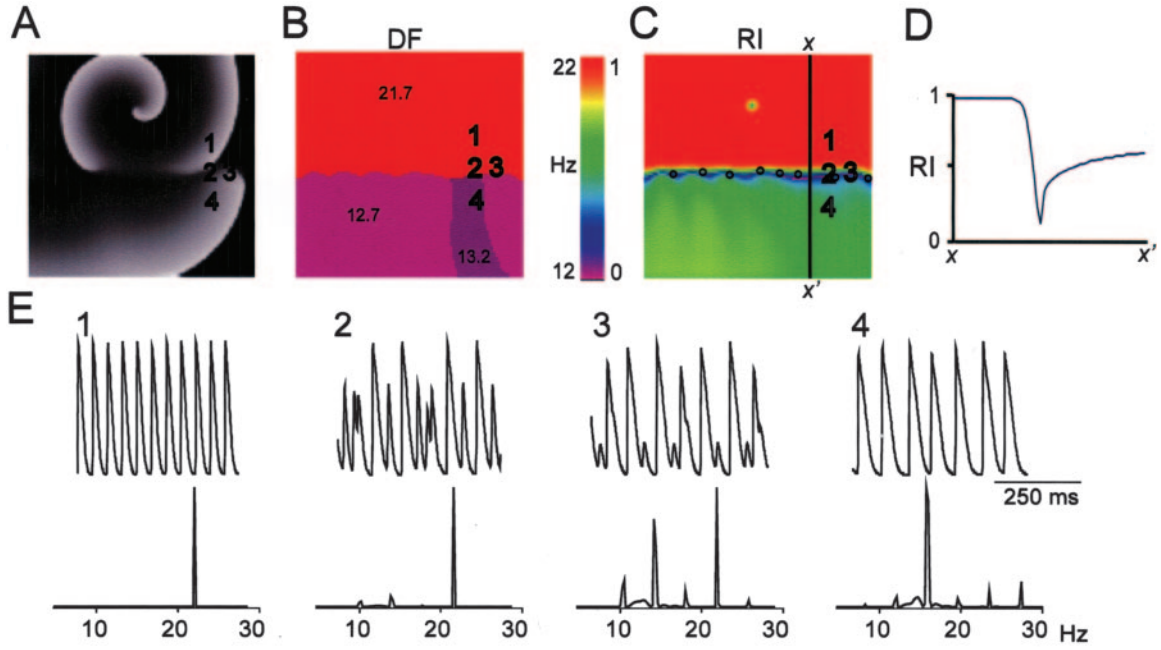

Figure 7. Numerical simulation. A, Snapshot of a fast and stable reentry in the upper half (high $I_{K,ACh}$), sending waves that block intermittently at interface with bottom half (low $I_{K,ACh}$). B, DF map. C, RI map. Region of highest DF (excluding the core) corresponds to the region of highest RI. At the border of the DFmax domain, a band of low RI is present. Circles indicate phase singularities. D, RI profile along the xx′ line in C. RI increases again in the low-frequency area (bottom half in A). E, Sample membrane potentials with corresponding power spectra from the DFax (1), interface (2 and 3), and lowest-DF (4) areas.

100%) and the variability of the conduction velocity is the lowest (conduction velocity, 0.36±0.001 m/s). In the band of high fractionation located between the DFmax and the low-DF domains (site 3), we observed large increases in the beat-to-beat variability of directionality (Figure 8B) and conduction velocity (RPD, 33%; conduction velocity, 0.22±0.122 m/s). Within the area of the low-DF domains (site 4), the variation of directionality (Figure 8C) and conduction velocity were smaller than in the high-fractionation band but still higher than in the DFmax domain (RPD, 56%; conduction velocity, 0.47±0.097 m/s).

Statement of Responsibility

The authors had full access to the data and take full responsibility for its integrity. All authors have read and agree to the manuscript as written.

Discussion

Major Findings

The major findings are as follows. First, during stable AF, the PLA harbors regular, fast, and spatiotemporally organized activity. Second, whether recorded optically or electrically, highly periodic impulses propagate repetitively from inside to outside the PLA and fractionate close to the outer limit of the DFmax domain. Third, the outer limit of the DFmax domain is the area where the most fractionated activity surrounds the most regular activity. Finally, the mechanism of wave fractionation during AF involves an increase in the beat-to-beat variability in the direction and conduction velocity of AF waves.

Relation Between Rate and Fractionation of AF Waves

Using a unique experimental approach to map the endocardial side of the PLA, we were able to visualize spatiotemporally organized activity and/or rotors in each experiment at frequencies and locations comparable to those recorded previously.[8,11,16,17] The high-frequency waves that emanate from breakthroughs at the PLA propagate in highly recurrent directions. We showed experimentally and numerically that the AF waves emanating from the DFmax area reach a boundary where they propagate intermittently, break, and change direction recurrently. The resulting signals (both optical and electric) analyzed by well-established criteria in the frequency[9,13] and time domains are clearly more fractionated outside the DFmax area. To the best of our knowledge, this is the first demonstration that fast and regular activity at the PLA is the cause of fractionation of wavefronts in its immediate surroundings.

Mechanism of AF Wave Fractionation

In both experiments (Figure 6B) and simulations (Figures 7 and 8), we show that the highest incidence of wavebreaks and beat-to-beat variability in the direction and velocity of propagation are associated with highly fractionated signals located at the boundaries of the DFmax domain. Note, however, that propagation direction and velocity may not be independent of each other and that, moreover, the change of any of them may be sufficient for the creation of local fractionated signals. For example, Fox et al[19] demonstrated that a periodic source propagating in a constant direction along a strand can result in local variability in transmembrane voltage amplitude and

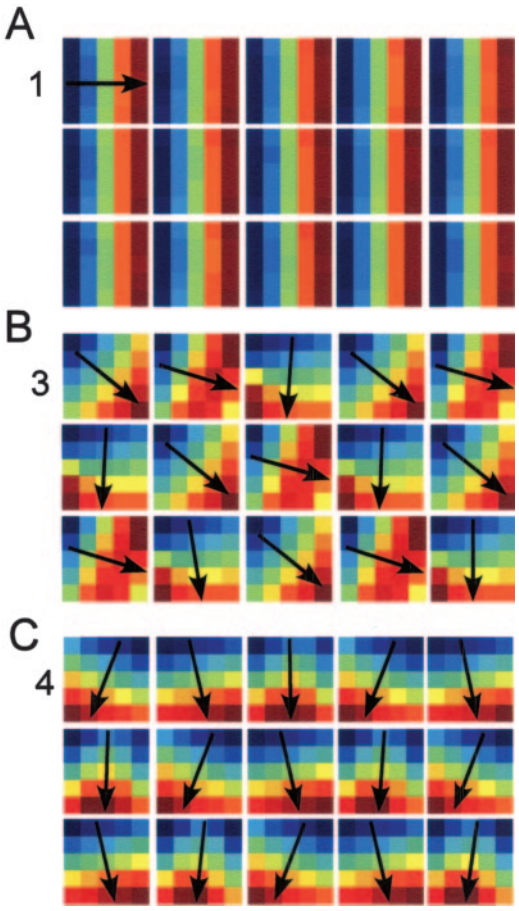

Figure 8. Directionality in numerical simulation. Vectorial best-fit analysis shows direction of propagation for 15 sequential (left-to-right, top-to-bottom) activations at pixels 1, 3, and 4 (see Figure 7). A, Pixel 1. No variability in directionality or conduction velocity (see text; area of highest DF and RI). B, Pixel 3. Maximum variability of directionality and conduction velocity (area of lowest RI). C, Pixel 4. Slightly reduced variability in conduction velocity and directionality (area of intermediate RI). Color scale is the normalized activation time from blue to red.

intermittent blockades. In addition, the shape of the impinging wavefront is likely to play a role in the homogeneity of the distribution of low RI values at the boundaries of the DFmax domain. This effect may explain the small differences between the DF and RI distributions on the right and left sides of the simulated maps in Figure 7. Indeed, Figure 7A shows that a reentrant wavefront approaches the boundaries between DF domains at slightly different angles on right versus left sides. In that regard, a hypothetical point source generating the activity would yield a slightly different RI distribution. Thus, the shape of the wavefront is an additional, albeit not independent, factor controlling fractionation.

Mechanisms of AF Maintenance

AF maintenance has been suggested to depend on organized microreentry, pacemaker, or triggered activity at the PLA.[8,10,11,20] The consistent observation of high frequency and spatiotemporally periodic waves in our experiments strongly supports the idea that AF in this model is maintained by functional reentry. The most common pattern of endocardial propagation in our study was that of a breakthrough, and the reentrant activity observed at the endocardium was short-lived. Previous epicardial recordings in isolated sheep hearts demonstrated that stable acetylcholine-induced AF was sustained by stable microreentrant sources located in the PLA wall near the PV ostia with an average core diameter <2 mm.[8] Thus, breakthroughs in our study are likely to have reflected reentry with an intramural filament.[21] Our simulation results also support the hypothesis that high-frequency reentry might very well be the mechanism supporting fractionation at DFmax domain boundaries. Nevertheless, we cannot completely exclude the possibility of another source mechanism. We chose to simulate reentry as an illustration of fast and stable source because, to the best of our knowledge, spontaneous pacemaker activity was not achievable at realistic experimental AF frequencies.

Clinical Implications

The PLA is known to play a critical role in maintenance of AF in patients.[1,5,22] Recently, electrogram-based radiofrequency ablation procedures have shown that frequency and/or fractionation criteria could be used to achieve satisfactory AF ablation success rates.[6,7] Nademanee et al[6] could terminate AF in a high percentage of patients by delivering radiofrequency at sites harboring fast CFAEs. However, other approaches such as the anatomic[3] and combined (anatomic and electrogram based[23]) methods have also proved effective. As such, the role of electrogram-based criteria of AF ablation has not been clearly established, and the electrophysiological mechanism and dynamics of fractionation of AF waves in patients have not been elucidated. Our experimental and numerical data describe the mechanism of fractionation of AF waves at the PLA. In fact, our results may help us to better understand the reason for the relatively high success rate of ablation procedures that use high-frequency CFAEs as the target for radiofrequency delivery.[6] Clearly, it would be erroneous to infer from the radiofrequency ablation data that the DFmax domain itself is the area of highest fractionation. In addition, our data also show that the site where most fractionation occurs during AF coexists in the periphery of the most rapid and less fractionated area. Therefore, we surmise that producing a relatively large anatomic obstacle by radiofrequency ablation in the region of high fragmentation that bounds the DFmax site would increase the likelihood of AF termination. This would happen because the ablation crater would form an effective wall against which the wavefront would collide head on and be annihilated. These new concepts introduce a new perspective in the clinical use of high-frequency CFAEs to localize sources of AF at the PLA and elsewhere.

Study Limitations

This study has a small size design ($n=8$). The properties of the substrate responsible for increased variability in velocity and direction of AF waves at the PLA have not been studied. It is reasonable to assume that the variability in direction of myocardial fibers[24,25] and other ionic properties at the PLA may have played a role. Finally, the fractionation properties of bipolar and unipolar recordings of the extracellular potential may be different from those of the transmembrane potential, as measured by optical mapping technique. However, data in Figure 2 and numerical simulations demonstrate

that the spatial relation between rate and fractionation holds regardless of the recording technique.

Acknowledgments

This work was supported by grants from the NHLBI (R01–HL–60843 to J.J.), Spanish Society of Cardiology (to F.A.), AHA postdoctoral fellowships (to J.K. and S.P.), and SDG (0230311N to O.B.). We thank Jianling Deng and Jiang Jiang for technical assistance.

Disclosures

None.

References

1. Jais P, Haissaguerre M, Shah DC, Chouairi S, Gencel L, Hocini M, Clementy J. A focal source of atrial fibrillation treated by discrete radiofrequency ablation. *Circulation*. 1997;95:572–576.
2. Haissaguerre M, Jais P, Shah DC, Takahashi A, Hocini M, Quiniou G, Garrigue S, Le Mouroux A, Le Metayer P, Clementy J. Spontaneous initiation of atrial fibrillation by ectopic beats originating in the pulmonary veins. *N Engl J Med*. 1998;339:659–666.
3. Pappone C, Oreto G, Rosanio S, Vicedomini G, Tocchi M, Gugliotta F, Salvati A, Dicandia C, Calabro MP, Mazzone P, Ficarra E, Di Gioia C, Gulletta S, Nardi S, Santinelli V, Benussi S, Alfieri O. Atrial electroanatomic remodeling after circumferential radiofrequency pulmonary vein ablation: efficacy of an anatomic approach in a large cohort of patients with atrial fibrillation. *Circulation*. 2001; 104:2539–2544.
4. Oral H, Knight BP, Tada H, Ozaydin M, Chugh A, Hassan S, Scharf C, Lai SW, Greenstein R, Pelosi F Jr, Strickberger SA, Morady F. Pulmonary vein isolation for paroxysmal and persistent atrial fibrillation. *Circulation*. 2002;105: 1077–1081.
5. Todd DM, Skanes AC, Guiraudon G, Guiraudon C, Krahn AD, Yee R, Klein GJ. Role of the posterior left atrium and pulmonary veins in human lone atrial fibrillation: electrophysiological and pathological data from patients undergoing atrial fibrillation surgery. *Circulation*. 2003;108:3108–3114.
6. Nademanee K, McKenzie J, Kosar E, Schwab M, Sunsaneewitayakul B, Vasavakul T, Khunnawat C, Ngarmukos T. A new approach for catheter ablation of atrial fibrillation: mapping of the electrophysiologic substrate. *J Am Coll Cardiol*. 2004;43:2044–2053.
7. Sanders P, Berenfeld O, Hocini M, Jais P, Vaidyanathan R, Hsu LF, Garrigue S, Takahashi Y, Rotter M, Sacher F, Scavee C, Ploutz-Snyder R, Jalife J, Haissaguerre M. Spectral analysis identifies sites of high-frequency activity maintaining atrial fibrillation in humans. *Circulation*. 2005;112:789–797.
8. Mandapati R, Skanes A, Chen J, Berenfeld O, Jalife J. Stable microreentrant sources as a mechanism of atrial fibrillation in the isolated sheep heart. *Circulation*. 2000;101:194–199.
9. Berenfeld O, Mandapati R, Dixit S, Skanes AC, Chen J, Mansour M, Jalife J. Spatially distributed dominant excitation frequencies reveal hidden organization in atrial fibrillation in the Langendorff-perfused sheep heart. *J Cardiovasc Electrophysiol*. 2000;11:869–879.
10. Arora R, Verheule S, Scott L, Navarrete A, Katari V, Wilson E, Vaz D, Olgin JE. Arrhythmogenic substrate of the pulmonary veins assessed by high- resolution optical mapping. *Circulation*. 2003;107:1816–1821.
11. Skanes AC, Mandapati R, Berenfeld O, Davidenko JM, Jalife J. Spatiotemporal periodicity during atrial fibrillation in the isolated sheep heart. *Circulation*. 1998; 98:1236–1248.
12. Samie FH, Berenfeld O, Anumonwo J, Mironov SF, Udassi S, Beaumont J, Taffet S, Pertsov AM, Jalife J. Rectification of the background potassium current: a determinant of rotor dynamics in ventricular fibrillation. *Circ Res*. 2001;89: 1216–1223.
13. Zaitsev AV, Berenfeld O, Mironov SF, Jalife J, Pertsov AM. Distribution of excitation frequencies on the epicardial and endocardial surfaces of fibrillating ventricular wall of the sheep heart. *Circ Res*. 2000;86:408–417.
14. Berenfeld O, Zaitsev AV, Mironov SF, Pertsov AM, Jalife J. Frequency-dependent breakdown of wave propagation into fibrillatory conduction across the pectinate muscle network in the isolated sheep right atrium. *Circ Res*. 2002;90: 1173–1180.
15. Kneller J, Zou R, Vigmond EJ, Wang Z, Leon LJ, Nattel S. Cholinergic atrial fibrillation in a computer model of a two-dimensional sheet of canine atrial cells with realistic ionic properties. *Circ Res*. 2002;90:E73–E87.
16. Mansour M, Mandapati R, Berenfeld O, Chen J, Samie FH, Jalife J. Left-to-right gradient of atrial frequencies during acute atrial fibrillation in the isolated sheep heart. *Circulation*. 2001;103:2631–2636.
17. Sarmast F, Kolli A, Zaitsev A, Parisian K, Dhamoon AS, Guha PK, Warren M, Anumonwo JM, Taffet SM, Berenfeld O, Jalife J. Cholinergic atrial fibrillation: I(K,ACh) gradients determine unequal left/right atrial frequencies and rotor dynamics. *Cardiovasc Res*. 2003;59:863–873.
18. Kalifa J, Jalife J, Zaitsev AV, Bagwe S, Warren M, Moreno J, Berenfeld O, Nattel S. Intra-atrial pressure increases rate and organization of waves emanating from the superior pulmonary veins during atrial fibrillation. *Circulation*. 2003;108: 668–671.
19. Fox JJ, Riccio ML, Hua F, Bodenschatz E, Gilmour RF Jr. Spatiotemporal transition to conduction block in canine ventricle. *Circ Res*. 2002;90:289–296.
20. Chou CC, Nihei M, Zhou S, Tan A, Kawase A, Macias ES, Fishbein MC, Lin SF, Chen PS. Intracellular calcium dynamics and anisotropic reentry in isolated canine pulmonary veins and left atrium. *Circulation*. 2005;111:2889–2897.
21. Pertsov AM, Jalife J. Scroll waves in 3 dimensional muscle. In: Zipes DP, Jalife J, eds. *Cardiac Electrophysiology, From Cell to Bedside*. Philadelphia, Pa: WB Saunders Co; 2000.
22. Lemery R, Guiraudon G. Catheter and surgical ablation strategies in atrial fibrillation: what have we learned? *Curr Opin Cardiol*. 2005;20:26–30.
23. Oral H, Knight BP, Ozaydin M, Chugh A, Lai SW, Scharf C, Hassan S, Greenstein R, Han JD, Pelosi F Jr, Strickberger SA, Morady F. Segmental ostial ablation to isolate the pulmonary veins during atrial fibrillation: feasibility and mechanistic insights. *Circulation*. 2002;106:1256–1262.
24. Hocini M, Ho SY, Kawara T, Linnenbank AC, Potse M, Shah D, Jais P, Janse MJ, Haissaguerre M, De Bakker JM. Electrical conduction in canine pulmonary veins: electrophysiological and anatomic correlation. *Circulation*. 2002;105: 2442–2448.
25. Nathan H, Gloobe H. Myocardial atrio-venous junctions and extensions (sleeves) over the pulmonary and caval veins: anatomical observations in various mammals. *Thorax*. 1970;25:317–324.

CLINICAL PERSPECTIVE

Radiofrequency catheter ablation is used in patients presenting drug-refractory atrial fibrillation (AF), with the goal of isolating and/or terminating the electrical sources responsible for the arrhythmia. Recent studies suggest that high-frequency complex fractionated atrial electrograms (CFAEs) recorded during AF could be used as target sites for ablation, as such sites may be important in the maintenance of AF. Nevertheless, it is not clear if there is any relationship between the fastest sites and the most fractionated sites, or what guidance can be obtained from their localization to improve ablation. In the present study, we use experimental and computer models of AF to explore the mechanism underlying signal fractionation during AF. We provide evidence that the fastest activity in the posterior left atrial wall of the sheep heart during AF is in fact the most regular, with most fractionated electrograms recorded in adjacent locations surrounding the AF sources. Our study demonstrates that AF-induced electrogram fractionation is the result of increased variability in propagation velocity and direction of waves emanating from AF sources. In addition, the waves fragment intermittently at the interface of the fastest region with areas of lower frequencies. Overall, these data help explain the high success rate of AF ablation techniques aimed at abolishing high-frequency CFAEs. It is likely that targeting high-frequency CFAEs for ablation results in isolation of the areas harboring the AF sources. As such, our results may open a new perspective in the treatment of AF in patients.

Mechanisms of Wave Fractionation at Boundaries of High-Frequency Excitation in the Posterior Left Atrium of the Isolated Sheep Heart During Atrial Fibrillation

Jérôme Kalifa, Kazuhiko Tanaka, Alexey V. Zaitsev, Mark Warren, Ravi Vaidyanathan, David Auerbach, Sandeep Pandit, Karen L. Vikstrom, Robert Ploutz-Snyder, Arkadzi Talkachou, Felipe Atienza, Gérard Guiraudon, José Jalife and Omer Berenfeld

Circulation. 2006;113:626-633
doi: 10.1161/CIRCULATIONAHA.105.575340
Circulation is published by the American Heart Association, 7272 Greenville Avenue, Dallas, TX 75231

Print ISSN: 0009-7322. Online ISSN: 1524-4539